https://doi.org/10.5194/bg-2022-188
Preprint. Discussion started: 25 October 2022
© Author(s) 2022. CC BY 4.0 License.

Biogeosciences Discussions Open Access EGU

Extracellular enzyme production in the coastal upwelling system off Peru during different upwelling scenarios: a mesocosm experiment

Kristian Spilling[1,2,*], Jonna Piiparinen[1], Eric P. Achterberg[3], Javier Arístegui[4], Lennart T. Bach[5], Maria T. Camarena-Gómez[1], Elisabeth von der Esch[6], Martin A. Fischer[7], Markel Gómez-Letona[4], Nauzet Hernández-Hernández[4], Judith Meyer[3], Ruth A. Schmitz[7], Ulf Riebesell[3]

1. Marine Research Centre, Finnish Environment Institute, Helsinki, Finland

2. Centre for Coastal Research, University of Agder, Kristiansand Norway

3. GEOMAR Helmholtz Centre for Ocean Research Kiel, Kiel, Germany

4. Instituto de Oceanografía y Cambio Global, IOCAG, Universidad de Las Palmas de Gran Canaria, Las Palmas de Gran Canaria, Spain

5. Institute for Marine and Antarctic Studies, University of Tasmania, Tasmania, Australia

6. Institute of Hydrochemistry, Chair of Analytical Chemistry and Water Chemistry, Technical University of Munich, Munich, Germany

7. Institute for General Microbiology, Christian Albrechts University Kiel, Germany

*corresponding author: kristian.spilling@syke.fi

https://doi.org/10.5194/bg-2022-188
Preprint. Discussion started: 25 October 2022
© Author(s) 2022. CC BY 4.0 License.


18 Abstract

19 The Peruvian upwelling system is a highly productive ecosystem that could be altered by
20 ongoing global changes. We carried out a mesocosm experiment off Peru, with the addition of
21 water masses from the regional oxygen minimum zone (OMZ) collected at two different sites
22 simulating two different upwelling scenarios. Here we focus on pelagic remineralization of
23 organic matter by extracellular enzyme production of leucine aminopeptidase (LAP) and alkaline
24 phosphatase activity (APA). After addition of the OMZ water, dissolved inorganic nitrogen (N)
25 was depleted, but the standing stock of phytoplankton was relatively high even after nutrient
26 depletion (mostly >4 µg chlorophyll *a* L^{-1}). During the initial phase of the experiment, APA was
27 0.6 nmol L^{-1} h^{-1} even though the PO_4^{3-} concentration was >0.5 µmol L^{-1}. Initially, the dissolved
28 organic phosphorus (DOP) decreased, coinciding with an increase in PO_4^{3-} concentration
29 probably linked to the APA. The LAP activity was very high with most of the measurements in
30 the range 200-800 nmol L^{-1} h^{-1}. This enzyme degrades amino acids, and these high values are
31 probably linked to the highly productive, but N-limited coastal ecosystem. Also, the experiment
32 took place during a rare coastal El Niño event with higher-than-normal surface temperatures,
33 which could have affected the enzyme production. Using a non-parametric multidimensional
34 scaling analysis (NMDS) with a generalized additive model (GAM), we found that
35 biogeochemical variables (e.g. nutrient and chlorophyll *a* concentrations), phytoplankton and
36 bacterial communities explained up to 64% of the variability in APA. The bacterial community
37 explained best the variability (34%) in LAP. The high hydrolysis rates for this enzyme suggests
38 that pelagic N remineralization supported the high standing stock of primary producers in the
39 mesocosms after N depletion.

40

https://doi.org/10.5194/bg-2022-188
Preprint. Discussion started: 25 October 2022
© Author(s) 2022. CC BY 4.0 License.


41

42 Introduction

43 The Peruvian upwelling system is one of the most productive marine ecosystems in the world
44 (FAO, 2018). Its high productivity is driven by the upwelling of deep, nutrient rich water that
45 fuels primary production when reaching the sunlit surface ocean. The fate of the biomass
46 produced is of great importance for higher trophic levels and biogeochemical cycles. The
47 primary limiting nutrient is nitrogen (N), but iron (Fe) availability is also an important driver for
48 phytoplankton biomass production in addition to light (Chavez et al., 2008; Messié and Chavez,
49 2015). Part of the phytoplankton biomass passes to higher trophic levels through grazing and
50 predation. As the upwelled water parcel is transported further offshore by Ekman transport, part
51 of the biomass settles out of the euphotic zone and is decomposed in intermediate water layers
52 creating an extensive oxygen minimum zone (OMZ; Kalvelage et al., 2013).

53 The ongoing warming of surface waters is projected to have several consequences on marine
54 ecosystems. For example, increasing temperatures lead to a reduction in gas solubility causing a
55 decrease in oxygen concentrations; warming will also increase thermal stratification and reduce
56 the ventilation of the deeper ocean (Keeling et al., 2010). Both of these effects will lead to
57 expanding OMZs with potential consequences for biogeochemical cycling (Oschlies et al.,
58 2018). Biogeochemical cycles of nitrogen (N) and phosphorus (P) are affected by O_2 depletions,
59 e.g. through denitrification and sediment P release (Canfield et al., 2005). Hence, expanding
60 OMZs may decrease the inorganic N : P ratio in the upwelled water potentially affecting the
61 seston (i.e. all suspended particles) stoichiometry and plankton community composition (Hauss
62 et al., 2012; Spilling et al., 2019).

https://doi.org/10.5194/bg-2022-188
Preprint. Discussion started: 25 October 2022
© Author(s) 2022. CC BY 4.0 License.


63 After inorganic nutrients (primarily N) have been depleted, the productive surface layer is driven
64 by recycled production. In this process, dissolved organic matter (DOM) must first be broken
65 down into simpler forms before the DOM elements become biologically available. The
66 decomposition of DOM is not a uniform process as it is affected by both abiotic and biotic
67 variables. Extracellular enzymes hydrolyze complex dissolved organic molecules and is the first
68 step in remineralization of these DOM elements (Arnosti, 2011). Quantifying the rates of pelagic
69 remineralization is important for understanding recycled production and element fluxes in the
70 uppermost water masses. There are a range of different enzymes that are used for hydrolyzing
71 DOM, and two of the most studied ones are Leucine aminopeptidase (LAP) and Alkaline
72 phosphatase (AP).

73 LAP is a protein degrading enzyme that is used extracellularly in aquatic systems by bacteria,
74 some phytoplankton and fungi (Hoppe et al., 1988; Stoecker and Gustafson, 2003; Gutiérrez et
75 al., 2011). It hydrolyses a broad spectrum of substrates with a free amino group, but it has
76 preference for N-terminal leucine and related amino acids (Burley et al., 1990).

77 The AP enzyme is produced by a wide range of different organisms including aquatic bacteria
78 and phytoplankton. Its main function is related to the hydrolysis of phosphate monoesters that
79 separate orthophosphate (PO_4) from an organic compound (Perry, 1972; Hoppe, 2003). AP exists
80 either as ectoenzyme (on the cell wall) or is excreted extracellularly and has for phytoplankton
81 commonly been related to P-limitation in aquatic environments (Rose and Axler, 1997; Nausch,
82 1998). Bacterial AP activity (APA) is more complex, as some, in particular particle attached
83 bacteria, take up and use C and N from the organic molecule after hydrolysis, and may for this
84 reason produce AP even under P replete conditions (Benitez-Nelson and Buesseler, 1999;
85 Hoppe, 2003; Labry et al., 2016).

https://doi.org/10.5194/bg-2022-188
Preprint. Discussion started: 25 October 2022
© Author(s) 2022. CC BY 4.0 License.


In this study, we were interested in the dynamics of LAP and APA after an upwelling event in relation to biogeochemical variables and communities of plankton and bacterioplankton, and our main aim was to understand how much of the variability in enzyme activities could be explained by biogeochemical variables (e.g. nutrient concentrations) and microbial communities. This was done during a mesocosm experiment set up off the coast of Peru.

Materials and methods

A detailed description of the mesocosm set up and collection and addition of deep-water can be found in Bach et al. (2020) within this special issue. In short, the mesocosm bags were 2 m in diameter and extended from the surface down to 19 m depth, where the last 2 m was a conical sediment trap. Eight mesocosm bags were used and they were moored at 12.0555°S; 77.2348°W just north of Isla San Lorenzo where the water depth is ~30 m. The mesocosms were closed by attaching the sediment trap to the bottom and pulling the top above the surface on 25 Feb, 2017. The bags were regularly cleaned from the inside and outside and sampled every second day with integrated water samplers (0-10 m depth, IWS, Hydro-Bios). For a full detailed sampling and cleaning timetable see Bach et al. (2020).

Water (100 m^3) from the oxygen minimum zone (OMZ) was collected from two locations. The first was collected on day 5 from 12.028323°S; 77.223603°W from 30 m depth, and the second one from 12.044333°S; 77.377583°W from 90 m depth. The original aim was to collect severe and moderate OMZ signature water (differing in e.g. nitrate concentrations) from the first and second site, respectively. This assumption was based on long-term monitoring data, however, the chemical properties (e.g. nitrate concentration) was more similar in these water masses than

https://doi.org/10.5194/bg-2022-188
Preprint. Discussion started: 25 October 2022
© Author(s) 2022. CC BY 4.0 License.


anticipated reflecting low and very low OMZ signatures from site 1 and 2 respectively, but this was discovered only after the collection. Deep-water was added to the mesocosms in two steps on day 11 and 12 after the enclosure of the mesocosms. Approximately ~20 m^3 of the mesocosm water was exchanged with OMZ water, and both deep-water stations were pumped into four replicate mesocosms. The water removed was pumped out from 11-12 m depth whereas the deep-water was pumped into carefully moving the input hose between 14-17 m depth. The water collected at 30 m depth was pumped into mesocosms M1, M4, M5 and M8 having low OMZ signature and deep-water from 90 m depth into mesocosms M2, M3, M6 and M7 having very low OMZ signature.

At the site of the mesocosms, the OMZ is close to the surface (<10 m depth; Graco et al., 2017) and consequently the bottom part of the mesocosm was low in oxygen. In order to keep the stratification inside the mesocosm we added 69 L of concentrated brine on day 13 by carefully inserting it between 12.5-17 m depth. The same procedure was repeated on day 33 when 33 L of brine was added. This artificial halocline prevented complete mixing of the mesocosm and the lower part of the mesocosm had a very different water chemistry compared to the upper 10 m. At the end of the experiment a third addition of brine was carried out to measure the total volume of the mesocosms.

Nutrient concentrations

Inorganic nutrients were determined from filtered (0.45 µm filter, Sterivex, Merck) samples immediately after the water arrived in the laboratory. For the measurements, we used a continuous flow analyzer (QuAAtro AutoAnalyzer, SEAL Analytical) connected to a

https://doi.org/10.5194/bg-2022-188
Preprint. Discussion started: 25 October 2022
© Author(s) 2022. CC BY 4.0 License.


fluorescence detector (FP-2020, JASCO). Phosphate (PO_4^{3-}), nitrate (NO_3^-) and nitrite (NO_2^-) were determined colorimetrically (Murphy and Riley, 1962; Morris and Riley, 1963) and corrected with the refractive index method reported by Coverly et al. (2012). Ammonium (NH_4^+) concentrations were determined fluorometrically (Kérouel and Aminot, 1997). Dissolved inorganic nitrogen (DIN) was calculated by summing NO_3^-, NO_2^- and NH_4^+. Further details on measurement accuracy can be found in Bach et al. (2020).

To measure total dissolved nitrogen (TDN) and phosphorus (TDP), the samples were first filtered through pre-combusted (5 h, 450°C) Whatman GF/F filters (pore size 0.7 µm). The filtrate was collected in 50 mL acid-cleaned high-density polyethylene (HDPE) bottles and placed directly into a freezer (-20°C). Later the filtrates were thawed at room temperature over a period of 24 hours and divided in two. The first half was used to determine inorganic nutrient concentrations as described above. From the other half we determined the TDN and TDP concentrations. An oxidizing reagent (Oxisolv, Merck) was added, and the samples were autoclaved for 30 minutes. TDN and TDP were measured spectrophotometrically (QuAAtro, Seal Analytical). Dissolved organic nitrogen (DON) concentrations were calculated by subtracting DIN from TDN. Dissolved organic phosphorus (DOP) was calculated as the difference between TDP and PO_4^{3-}.

Fluorescent dissolved organic matter and PARAFAC analysis

Fluorescent dissolved organic matter (FDOM) was determined by measuring fluorescence in water samples with a Cary Eclipse (Agilent Technologies) spectrofluorometer, using excitation

https://doi.org/10.5194/bg-2022-188
Preprint. Discussion started: 25 October 2022
© Author(s) 2022. CC BY 4.0 License.


and emission slit widths of 10 nm. Wavelength ranges were set to 230-456 nm for excitation, with 2 nm increments, and the 290-600 nm for emission with 5 nm increments. The measurements were collected into excitation-emission matrices (EEM). Blanks were measured with the same settings using ultrapure water.

Raw measurements were processed using the DOMFluor toolbox (v. 1.7; Stedmon and Bro, 2008) for Matlab (R2017a). The processing consisted in 1) blank subtraction from seawater EEMs, 2) EEMs normalization to the Raman area (RA), estimated applying the trapezoidal rule of integration on the emission scan at the 350 nm excitation wavelength in the blank EEMs, and 3) cropping of the 1st and 2nd order Rayleigh scatter bands. Inner filter correction was not performed as for the duration of the experiment the absorption coefficient at 250 nm (a250) displayed values (mean ± sd = 1.56 ± 0.91 m^{-1}) well below 10 m^{-1}, above which correction is considered necessary (Stedmon and Bro, 2008).

The processed EEMs were analyzed applying a Parallel Factor Analysis (PARAFAC) using the DOMFluor toolbox. The PARAFAC model was constructed based on 125 samples (outliers were removed) and validated using split-half validation and random initialization. The resulting model consisted of 4 components (C1-C4; supplementary material Fig S1). For each of them, the fluorescence maximum (Fmax) was recorded. The identified fluorophores were compared to others found in the literature using the OpenFluor database (openfluor.lablicate.com; Murphy et al., 2014).

https://doi.org/10.5194/bg-2022-188
Preprint. Discussion started: 25 October 2022
© Author(s) 2022. CC BY 4.0 License.


Phytoplankton community and chlorophyll a

Flow Cytometry subsamples were transferred from the IWS into 50 mL beakers and stored cool in the dark until analysis max. 8 hours after sampling. Each sample (650 µL) was analyzed with an Accuri C6 flow cytometer (BD Biosciences) set to a high flow rate (i.e. 66 µL/min). Phytoplankton groups were differentiated based on the strength of the forward scatter (FSC-A), the side scatter (SSC-A), the red fluorescence (FL3-A) and orange fluorescence (FL2-A) signal ("A" refers to the area of the signal integral). Furthermore, we used sequential filtrations with different polycarbonate filters (Whatman, pore-sizes 0.2, 0.4, 0.8, 2, 3, 5, 8 µm) to distinguish populations in the cytogram based on size. This procedure was helpful to approximate how FSC-A values corresponded with size. We defined the following phytoplankton groups: Synechococcus-like cells (Syn; 0.2-2µm), Cryptophyte-like cells (Crypto; ~90% between 2-5 µm), picoeukaryotes (Peuks; 0.2-2 µm), Nanoeukaryotes (Nano; 2-20 µm, mostly in the lower range), Microeukaryotes 1 (Mikro1; ~15-40 µm, occasionally overlapping with Nano), Microeukaryotes 2 (Mikro2; ~>40 µm, cluster dominated by *Akashiwo sanguineum* from about day 20 onward), elongated cells "chains" determined by the ratio of FSC-A to FSC-H where "H" refers to the height of the forward scatter signal (details about this approach are provided in Paul et al., this issue. The goal of this was to detect chain-forming diatoms which we expected to be an important component of the community).

Samples for chlorophyll *a* (chl-*a*) determination were filtered onto GF/F filters (Whatman) and flash frozen in liquid nitrogen and stored at -80 °C (or dry ice for a brief period during air transfer; ~2 days) until measurement. The chl-*a* concentration was measured using high-performance liquid chromatography. The chl-*a* autofluorescence of the phytoplankton community was measured with a handheld fluorometer (AquaPen, Photon Systems Instruments)

https://doi.org/10.5194/bg-2022-188
Preprint. Discussion started: 25 October 2022
© Author(s) 2022. CC BY 4.0 License.


using 450 nm excitation light. The photochemical efficiency was calculated based on the relationship between the variable to maximal fluorescence (Fv/Fm).

16S-rRNA gene based bacterial community determination

One liter of surface water obtained from the individual sampling sites was filtered through sterile Millipore Express PLUS membrane filters (polyethersulfon) with a cut-off of 0.22 µm and a diameter of 47 mm (Merck Millipore). After filtration, the filters were flash frozen in liquid nitrogen and stored at -80°C until nucleic acid extraction. Nucleic acid extraction was performed using the NucleoSpin TriPrep- Kit (Machery-Nagle) according to manufacturer's instruction with an additional step at the beginning of the extraction using a pestle to properly homogenize the sample.

Primers applied for the amplification of the bacterial 16S rRNA gene fragments were annealing to the variable region 1 and 2 and consisted of an initial standardized Illumina adapter (regular), followed by an 8 nucleotide barcode (X's), a linker region (underlined) and a primer sequence (bold). The sequences were for the forward primer Bac27 5'-AATGATACGGCGACCACCGAGATCTACACXXXXXXXXTATGGTAATTGT**AGAGTTT GATCCTGGCTCAG**-3' and reverse Bac338 5'-CAAGCAGAAGACGGCATACGAGATXXXXXXXXAGTCAGTCAGCC**TGCTGCCTCCC GTAGGAGT**-3'. The individual PCR reaction contained 100 ng of the extracted DNA. PCR conditions and purification of the amplification product were previously described (Fischer et al. 2019a). The final library pool for sequencing was combined from the eluates and contained 100 ng of DNA. Amplicon library sequencing was performed on a MiSeq instrument. Library

https://doi.org/10.5194/bg-2022-188
Preprint. Discussion started: 25 October 2022
© Author(s) 2022. CC BY 4.0 License.


217 therefore was prepared according to the manufacturer's instructions and sequenced using the v3
218 chemistry with 2 x 300bp paired-end.

219 Reads generated with amplicon sequencing were trimmed using the trimmomatic software
220 version 0.33 (Bolger et al., 2014) as described in Fischer et al. (2019b). Briefly, reads were
221 analyzed with a sliding window of 4 bp and regions were trimmed if the average Phred score
222 (Ewing and Green, 1998; Ewing et al., 1998) within the window was below 30. Trimmed reads
223 were kept within the dataset if the forward and reverse read both survived the quality trimming
224 and were longer than 36 bp. Afterwards, 20,000 reads per sample were kept in the dataset
225 (exceptions were sample M1 on day 10 (5817 reads) and M7 on day 24 (17660 reads) for further
226 analysis.

227 Quality trimmed sequences were analyzed using MOTHUR software, version 1.35.1 (Schloss et
228 al., 2009) as described in Fischer et al. (2019a). The quality filtered and subsampled reads were
229 concatenated to 1,040,321 contiguous sequences (contigs) using the command make.contig.
230 Contigs were filtered for ambiguous bases, homopolymers longer than 8 bases or sequences
231 longer than 552 bases using the command screen.seqs. The resulting 754,310 contigs were
232 checked for redundant sequences using the command unique.seqs and clustered to 199,746
233 unique sequences. The sequences were consecutively aligned to a modified version of the
234 SILVA database release version 132 (Pruesse et al., 2012) containing only the hypervariable
235 regions V1 and V2 by the command align.seqs. Sequences not aligning in the expected region
236 were removed from the dataset using the command screen.seqs. The alignment was further
237 optimized by removing gap-only columns with the command filter.seqs. The alignment
238 contained 717,217 sequences (148,760 unique). Rare and closely related sequences were
239 clustered using the commands unique.seqs and precluster.seqs. The latter was used to cluster

https://doi.org/10.5194/bg-2022-188
Preprint. Discussion started: 25 October 2022
© Author(s) 2022. CC BY 4.0 License.


sequences with up to 3 positional differences compared to larger sequence clusters together. Chimeric sequences were removed using the implemented software UCHIME (Edgar et al., 2011) using the command chimera.uchime, followed by remove.seqs leaving 551,142 sequences (29,519 unique) in the dataset. The classification of the sequences was performed against the SILVA database and was done with a bootstrap threshold of 80 %. Operational taxonomic units (OTUs) were formed using the average neighbor clustering method with the command cluster.split. A sample-by-OUT table on the 97 % level, containing 10,258 OTUs, was generated using the command make.shared. These OTUs were used for the subsequent analysis. After the removal of mitochondria, chloroplast and singletons, 3225 OTUs were retained. These OTUs were used for downstream analysis.

Extracellular enzymes

The leucine aminopeptidase (LAP) activity was determined using the method described by Stoecker and Gustafson (2003) using *L*-leucine 7-amido-4-methyl-coumarin (Leu-AMC; Sigma Aldrich) as a substrate. Leu-AMC was added to a final concentration of 500 µmol L^{-1}, which was determined in separate kinetics tests to saturate the enzyme activity. The samples (100-200 µl) were incubated in the dark at in situ surface temperature for a minimum of four hours. The fluorescence was measured every 30-60 min with a Cary Eclipse (Agilent Technologies) spectrofluorometer using 380 nm excitation and 440 nm emission wavelengths. The results were compared with a standard curve determined using 7-amino-4-methyl-coumarin (AMC; Sigma Aldrich) dissolved in DMSO, and the LAP activity calculated by linear regression.

https://doi.org/10.5194/bg-2022-188
Preprint. Discussion started: 25 October 2022
© Author(s) 2022. CC BY 4.0 License.


Measurements of alkaline phosphatase activity (APA) were conducted with 20 ml subsamples of initial/incubated seawater using 100 nmol L^{-1} 4-methylumbelliferyl phosphate (MUF-P; Sigma-Aldrich) as the organic phosphate substrate (Ammerman, 1993). Fluorescence was measured on a BIOTEK Microplate Reader with a Cary Eclipse (Agilent Technologies) spectrofluorometer using 355 nm excitation light and 460 nm emission detection. Following MUF-P addition, fluorescence measurements were performed at 0, 1.5, and 3 h and APA (h^{-1}) was calculated from the linear increase in fluorescence and calibrated against 4-methylumbelliferone (MUF; Sigma-Aldrich). The assays were performed and incubated in the dark. Ultrapure water (Milli-Q) blanks and paraformaldehyde-killed controls generally yielded fluorescence values similar to *t* = 0 readings.

Statistical analysis

Before comparisons between the two experimental treatments were conducted, we first constructed a cumulative value where each measured value was summed up for each sampling day. The linear regressions of the cumulative enzyme activity from the two treatments (n = 4) were compared with Student's t-test. In addition, the effect of biogeochemical, phytoplankton and bacterioplankton community composition to APA and LAP was determined, using the ordination scores of the first and second axis of a non-parametric multidimensional scaling (NMDS) as explanatory variables in generalized additive models (GAMs) with APA or LAP as dependent variable. The NMDS was applied separately to each group of variables: biogeochemical, phytoplankton community and bacterioplankton community. The individual

https://doi.org/10.5194/bg-2022-188
Preprint. Discussion started: 25 October 2022
© Author(s) 2022. CC BY 4.0 License.


explanatory power of each MDS score was estimated with a univariate GAM. The visualization of the links was done for each explanatory variable through the prediction from the full model object, setting all other explanatory variables at their mean value. In addition, links to the scores of the biogeochemical variables and phytoplankton community NMDS were estimated with one GAM model. It was not possible to include the bacterioplankton community into this model due to the different sampling regime (lower number of samples) and this was treated with a second model. NMDS was estimated with the metaMDS function in the Vegan package (Oksanen et al., 2019), and GAMs were fitted using the gam function in the mgcv package (Wood, 2017). For explaining the deviance, an adjusted coefficient of determination (R^2) was used. An adjusted R^2 takes into account the model complexity and is more conservative than a non-adjusted R^2.

RESULTS

Nutrients

The addition of deep-water increased the phosphate concentrations whereas the dissolved inorganic nitrogen (DIN) was >2 µmol L^{-1} in the mesocosms until after the addition of deep-water (days 11 and 12 of the experiment). After the addition of the deep-water, the DIN concentration rapidly declined and was depleted at day 15 in most mesocosms except in M3 where DIN depletion occurred a week later (day 22; Fig 1). The PO_4^{3-} concentration increased after closing the mesocosm and reached ~1.9 µmol L^{-1} in all mesocosms after the deep-water

https://doi.org/10.5194/bg-2022-188
Preprint. Discussion started: 25 October 2022
© Author(s) 2022. CC BY 4.0 License.


addition. There was only a slight reduction to approximately 1.5 µmol PO_4^{3-} L^{-1} over the course of the experiment (Fig 1).

The dissolved organic nitrogen (DON) and phosphorus (DOP) concentrations were initially 9 – 12 µmol L^{-1} and 0.6 – 1.0 µmol L^{-1}, respectively. There was no drastic change in DON with the deep-water addition and there was an overall decrease in DON to 6.0 - 7.9 µmol L^{-1} on day 30 after which it increased somewhat again. The DOP concentrations decreased rapidly the first 8 days to 0.19 - 0.32 µmol L^{-1} but increased after the deep-water addition and remained within 0.2 - 0.7 µmol L^{-1} interval for the rest of the experiment.

The PARAFAC modelling of the EEMs yielded four FDOM components (C1-C4; Fig 2, Fig S1). Using the OpenFluor database we identified multiple fluorophores with strong similarity (TCCex·em > 0.95) to our components (Table S1). Components 1 and 3 had characteristics resembling amino acid/protein compounds whereas components 2 and 4 were more humic-like (Table S1). All FDOM components increased sharply at day 18. This did not take place in Pacific seawater sampled outside the mesocosm where the FDOM was relatively stable throughout the experiment. After the increase at day 18, humic-like components (C2 and C4) were relatively stable but decreased slightly after day 28-30. The amino acid-like components (C1 and C3) exhibited higher variability among mesocosms, and C3 had overall higher variability throughout the experiment. Both humic-like and amino acid-like components maintained fluorescence values above the initial ones until the end of the experiment, but there were no clear differences between the treatments. However, towards the end of the experiment M1 and M2 had highest concentrations of C1, M1 also had highest concentration of C2 and C3 whereas M3 had the highest concentration of C4 at the end of the experiment.

https://doi.org/10.5194/bg-2022-188
Preprint. Discussion started: 25 October 2022
© Author(s) 2022. CC BY 4.0 License.


324

325 Chlorophyll, photochemical efficiency and phytoplankton community

326 After deep-water addition, the chl-*a* concentration increased from 2-4 µg L^{-1} to 4-8 µg L^{-1} except
327 for mesocosms M3 and M4 where the increase was not as pronounced (Fig 3). The chl-*a*
328 concentration in M3 increased after day 22 to ~4 µg Chl-*a* L^{-1}, whereas in M4 the chl-*a*
329 concentration remained low (<2 µg L^{-1}) throughout most of the experiment (Fig 3). The
330 photochemical efficiency (Fv/Fm) was approximately 0.7 throughout the whole experiment
331 without major difference between mesocosms, except for M4 where it was consistently lower
332 (<0.6) during the last week of experiment (Fig 3).

333 The initial community was dominated by diatoms in terms of biomass but this group gradually
334 reduced in numbers after the enclosure of the mesocosms and instead the mixotrophic
335 dinoflagellate *Akashiwo sanguineum* appeared (Fig 4). The cell counts done with the flow
336 cytometer were checked with a microscope and this was the primary species in terms of biomass
337 in the Microeukaryote 2 group (Fig 4). The exceptions were mesocosms M3 and M4 where this
338 dinoflagellate was not abundant (M4) or bloomed later (M3) and where there were more
339 Chrysophytes. In M4 there was in addition a bloom of picoeukaryotes starting after day 20 (Fig
340 4).

341

342 Bacterial community

343 The bacterial community was dominated by the class Alphaproteobacteria throughout the whole
344 experiment and in all the mesocosms units, reaching values between 60 to 88% of the total

https://doi.org/10.5194/bg-2022-188
Preprint. Discussion started: 25 October 2022
© Author(s) 2022. CC BY 4.0 License.


345 sequences at day16 (Fig 5). Within Alphaproteobacteria, the *Roseobacter* lineage (genera
346 HIMB11, *Ascidiaceihabitans*, *Amylibacter* and *Planktomarina* in M1) of the order
347 Rhodobacterales contributed most to the bacterial community in all the mesocosms (10-55 %) in
348 particular on day 16, except in M8 where the SAR11 Ia clade dominated the community (55% of
349 the total sequence at day 16). The order Parvibaculales had high relative abundances (12-20% of
350 the total sequences) in M4, M5, M6 and M7 before the deep-water addition (day 10) decreasing
351 in the following week. The relative abundance of order Rickettsiales peaked at day 16 in all the
352 mesocosms except in M8, decreasing after one week. The class Gammaproteobacteria comprised
353 between 20 to 45% of the total relative abundance. Within Gammaproteobacteria, the order
354 Thiomicospirales had high relative abundance (8-17% total sequences) at day 10 in most of the
355 mesocosms, whereas the order Cellvibrionales and order Oceanospirillales (genus
356 *Pseudohongiella*) increased from day 24 and by the end of the experiment, respectively. In M8,
357 the abundances of orders Thiomicospirales and Pseudomonadales (14% of total sequences)
358 increased at day 24. Other groups that increased in abundance in the second half of the
359 experiment were the deltaproteobacterial orders Desulfobacteriales (7-20% in M2, M3, M4 and
360 M5) and Bdellovibrionales (5-8% in M2, M3 and M4). The order Flavobacteriales dominated
361 within Bacteroidetes and the relative abundance ranged from 1 to 25% throughout the
362 experiment, being generally high (10-20%) at day 10 . The flavobacterial genus *Aurantivirga*
363 contributed > 7% in M1, M2 and M3.

364

365 Enzyme activity

https://doi.org/10.5194/bg-2022-188
Preprint. Discussion started: 25 October 2022
© Author(s) 2022. CC BY 4.0 License.


366 The initial LAP activity before the deep-water addition was relatively low (average 359 nmol L^{-1}
367 h^{-1} ± 81 nmol L^{-1} h^{-1} SD) but increased after the addition of deep-water in some of the
368 mesocosms (Fig 6). In M3 the LAP activity was high, reaching 1600 nmol L^{-1} h^{-1} directly after
369 the deep-water addition, but decreased after that. The highest cumulative LAP activity at the end
370 of the experiment was in M7 where the LAP activity was 716 nmol L^{-1} h^{-1} after deep-water
371 addition and the average after day 16 was 657 nmol L^{-1} h^{-1} ± 142 nmol L^{-1} h^{-1} (SD). There was a
372 difference between the treatments in the cumulative LAP after the addition of the deep-water
373 until day 16, with the very low OMZ signature (lowest NO_3 concentration) water producing the
374 highest LAP activity (Students' t-test, $p = 0.047$), but this difference disappeared after day 16 (p
375 $= 0.44$).

376 The alkaline phosphatase activity (APA) was 0.5-0.6 nmol L^{-1} h^{-1} at the beginning of the
377 experiment but decreased to undetectable levels after day 30 (Fig 7). There was a noticeable drop
378 in APA after the addition of the deep-water, and the decrease continued gradually until day 28
379 after which the APA was very low (<0.1 nmol L^{-1} d^{-1}). The APA was similar in all the
380 mesocosms and there was no treatment effect ($p = 0.81$). The exception to this was M3 where the
381 APA was lower, compared to all other mesocosms for most of the experiment (Fig 7).

382 The variability in APA was better explained by the measured variables than LAP (Fig 8). The
383 biogeochemical variables and bacterioplankton community separately explained 62% of the
384 variability in APA, whereas the phytoplankton community alone explained 57% of the
385 variability. Combining both the biogeochemical variables and the phytoplankton community
386 increased the explanatory power to 74% (bacterioplankton community not included as the
387 number of sample points were less). The variability in LAP was best explained by the
388 bacterioplankton community (38%) followed by biogeochemical variables (20%) and

https://doi.org/10.5194/bg-2022-188
Preprint. Discussion started: 25 October 2022
© Author(s) 2022. CC BY 4.0 License.


389 phytoplankton community (18%). The combined biochemical variables and phytoplankton
390 community explained 28% of the LAP variability.

391

392

393 DISCUSSION

394 After the closure and addition of deep-water there was rapid phytoplankton growth in the upper 5
395 m of the mesocosms, with low light conditions limiting primary production deeper down (Bach
396 et al., 2020). The DIN concentrations were depleted around day 18 coinciding with an increase in
397 several of the FDOM components (both amino acid-like and humic-like components), also
398 matching the end of the phytoplankton bloom. There was, however, relatively constant and low
399 export of carbon out from the mesocosms (Bach et al., 2020) and at the same time relatively high
400 Chl-*a* concentration (mostly >4 µg chl-*a* L^{-1}) under conditions with depleted DIN (Fig 3). In
401 addition, the photochemical efficiency was overall relatively high (>0.5) throughout the
402 experiment suggesting regenerated primary production driven by recycling of nutrients. The
403 measured hydrolysis rates, particularly LAP, indicated that extracellular enzyme activity plays an
404 important role for this recycled production.

405 The main aim of this study was to relate the biogeochemical and microbial community to the
406 extracellular enzyme activity and a more detailed description of the temporal development and
407 biomass comparison of microbial groups will be presented elsewhere in this special issue (e.g.
408 Bach et al., 2020). Among phytoplankton, diatoms are typically dominating following upwelling
409 events (Anabalón et al., 2016), whereas dinoflagellates tend to become more dominant after

https://doi.org/10.5194/bg-2022-188
Preprint. Discussion started: 25 October 2022
© Author(s) 2022. CC BY 4.0 License.


410 establishment of stratification (Margalef et al., 1979). This was also seen in our mesocosm as the
411 dinoflagellate *Akashiwo sanguinea*, a mixotrophic species that may form red tides (Jeong et al.,
412 2005; Badylak et al., 2014), that quickly appeared in most mesocosm after OMZ water was
413 added with some exceptions. In M3 it appeared a little later and in M4 it did not bloom at all.
414 Interestingly these two mesocosms had a higher concentration of cryophytes and M4 had
415 additionally a bloom event of picoeukaryotes. Being mixotrophic, *A. sanguinea* is known to prey
416 on smaller species (Jeong et al., 2005) and lower grazing pressure could be the reason for the
417 bloom of picoeukaryotes in M4.

418 The bacterial community composition changed during the experiment but without clear treatment
419 effects. The dominant bacterial groups were the class Alphaproteobacteria, (Parvibaculales,
420 SAR11 subclade Ia, Roseobacter clade and Rickettsiales), class Gammaproteobacteria (SAR116
421 clade, Cellvibrionales, Oceanospirillales and SUP05 clade) and to lesser extent the class
422 Deltaproteobacteria (Desulfobacterales) and class Bacteroidea (order Flavobacteriales). SAR11
423 subclade Ia, Roseobacter clade, SAR116 clade, SUP05 clade and Desulfobacterales are known to
424 utilize inorganic and organic sulfur components such as hydrogen sulfide (H_2S), sulfate (SO_4)
425 and dimethylsulfoniopropionate (DMSP) metabolites for their metabolic requirements (Nowinski
426 et al., 2019) and are coupled with the nitrogen cycle (Schunck et al., 2013). Specifically, the
427 sulfur-oxidizing SPU05 oxidizes H_2S coupled with the nitrate reduction and potentially produces
428 nitrite (Shah et al., 2017), whereas Desulfobacterales play an important role in N_2 fixation (Gier
429 et al., 2016). These bacterial taxa associated with the sulfur cycle are typically found in the OMZ
430 regions (Pajares et al., 2020). We observed a temporal shift in the bacterial community through
431 the experiment changing between sulfur-oxidizing (SUP05) and sulfate-reducing
432 (Desulfobacterales) bacteria, probably liked to the nitrate availability, i.e. more DIN at the

https://doi.org/10.5194/bg-2022-188
Preprint. Discussion started: 25 October 2022
© Author(s) 2022. CC BY 4.0 License.


433 enclose of the mesocosms and thus more relative abundance of SUP05. We also observed a shift
434 within phytoplankton-associated bacteria (*Roseobacter* lineage, Gammaproteobacteria, and
435 Flavobacteriales) that likely responded to the availability of DOM supply during the experiment
436 (Buchan et al 2014, Chafee et al 2017). The high relative abundance of Flavobacteriales and
437 genera from the *Roseobacter* lineage on days 10 and 16, respectively, coincided with the increase
438 in chl-*a* and high LAP activity until day 16. Positive correlations have been observed between
439 chl-*a*, Bacteroides and Deltaproteobacteria and LAP during phytoplankton blooms (Shi et al
440 2019). However, we do not have gene expression data and cannot make any firm conclusion
441 about the connection between these groups and production of LAP.

442 The temporal shift in the bacterial community indicates niche partitioning between bacterial taxa
443 that assimilate different organic substrates or inorganic sulfur components, produced during
444 phytoplankton bloom events or from sulfidic events (Schunck et al., 2013; Callbeck et al., 2018;
445 Nowinski et al., 2019). Our results support previous studies that have demonstrated the important
446 role of the sulfur cycle in shaping the bacterial community composition in poorly oxygenated
447 waters (Schunck et al., 2013; Aldunate et al., 2018). It is worth to note that the conditions in the
448 bottom of the mesocosms were sub-oxic and there might have been a clear depth gradient in the
449 bacterial community that was not picked up by our integrated 0-10 m sampling.

450 Overall, there was a treatment effect of the different OMZ waters on the LAP activity, with
451 higher LAP in the very low OMZ signature addition, but this effect was only observed right after
452 the addition of the deep-water. There were also slightly higher NO_3 concentrations in this water
453 (Bach et al., 2020). However, this difference in both DIN and LAP was relatively small and
454 disappeared a week after the OMZ water addition, most likely because the collected deep-water
455 were more similar between the two locations than anticipated, with relatively similar

https://doi.org/10.5194/bg-2022-188
Preprint. Discussion started: 25 October 2022
© Author(s) 2022. CC BY 4.0 License.


456 concentrations of DIN. Although there were differences between individual mesocosms in terms
457 of the plankton community structure, there were no clear differences between treatments, and we
458 can conclude that the availability of nutrients by itself can shift the LAP production.

459 The LAP activity in our study was very high (~10-times higher compared with most literature
460 data). In a comparable study but further offshore in Peru, the LAP activity was 20 – 65 nmol L^{-1}
461 h^{-1} in surface waters (Maßmig et al., 2020). Further to the south, in Chile (30° 30.80' S), values
462 up to 230 nmol L^{-1} h^{-1} have been recorded, with a clear seasonal cycle linked to upwelling events
463 (Gutiérrez et al., 2011). With most of our data ranging between 200 – 800 nmol L^{-1} h^{-1} it is clear
464 that these LAP activities are linked to the upwelling, which is more intense near the coast and
465 also more constant at the study site compared with further south. The enzyme activity in
466 sediments can be up to three orders of magnitude higher than what we found (Hoppe et al.,
467 2002), and an order of magnitude higher values have been observed in a eutrophic, salt-water
468 lake (Song et al., 2019). The high LAP activities are likely a reflection of the high microbial
469 activity in the Peruvian upwelling system. The experiment was also taking place during a rare
470 coastal El Niño event (Garreaud, 2018), with anomalous higher surface temperatures, which
471 could be a reason for the high values we recorded as LAP is known to increase with temperature
472 (Christian and Karl, 1995).

473 There was also some loss of N due to denitrification, estimated to 0.2-4.2 nmol N_2 L^{-1} h^{-1} during
474 the experiment (Schulz et al 2021). For comparison, the LAP activity suggests an average of 417
475 nmol L^{-1} h^{-1} hydrolyzation of N-containing compounds, but this should be seen as the maximal
476 potential rather than the actual rate. The use of fluorescently labelled substrates for measuring
477 extracellular activity is a proxy method that has some drawbacks. The primary one is that the
478 molecular structure of the substrate used is never equivalent to the high molecular weight DOM

https://doi.org/10.5194/bg-2022-188
Preprint. Discussion started: 25 October 2022
© Author(s) 2022. CC BY 4.0 License.


in the water. This means that the measured hydrolysis rates could be an overestimation of the actual hydrolysis rates of DOM (e.g. Arnosti, 2011). The primary benefit of the method is that it is straightforward and has been in widespread use for decades, which means that comparisons with other ecosystems is possible, and for our purpose, we can use it for better understanding how much of the variability can be explained by the other measured variables.

Considering the APA, the most interesting aspect was that it was measurable in the beginning of the experiment at high PO_4^{3-} concentration. This high APA activity at high PO_4^{3-} concentration has been observed in deep oceans (Hoppe and Ullrich, 1999; Baltar et al 2016). Baltar and collaborators (2016) also observed an increase in APA in experiments amended with organic matter suggesting the activity of APA by organic matter supply, independently of the PO_4^{3-} concentration. This could be due to bacterial APA, which is more complex than for phytoplankton, in that it can be linked to the hydrolysis and acquisition of C (Hoppe, 2003). This is supported by the initial decrease in DOP and increase in PO_4^{3-}, which indicates that the AP hydrolysis of DOP added to the PO_4^{3-} pool. It is known that APA stays suspended and active for a long time in marine environments, and cell-free APA was reduced by only 25% over 16 days in the experiment by Thomson et al. (2019). If this enzyme is viable for this long, it suggests that there was no new production of AP after the closure of the mesocosms, which is supported by the dilution effect of adding the deep-water. In that case, the disappearance of the initial AP took 30 days.

The hydrolysis rates of AP were relatively low compared with most published data, probably linked to the clear surplus of PO_4^{3-}. It is worth to note, however, that we were most likely not

https://doi.org/10.5194/bg-2022-188
Preprint. Discussion started: 25 October 2022
© Author(s) 2022. CC BY 4.0 License.


measuring the maximal potential hydrolysis rates as substrate addition was relatively low (100 nmol L^{-1}) and would likely have been higher with more added substrate. This could be the reason for the apparent discrepancy between the measured hydrolysis rates and the change in the PO_4^{3-} and DOP pools during the 10 first days of the experiment. During this time there was a decrease of approximately 0.5 µmol DOP L^{-1} and an increase of 0.6 µmol PO_4^{3-} L^{-1}, suggesting an actual hydrolysis rate of 2.0-2.5 nmol L^{-1} h^{-1} (assuming 500-600 nmol over 10 days). This is a factor 3-4 higher compared with the initially measured APA of ~0.6 nmol L^{-1} h^{-1}.

The statistical model that we applied was better at explaining the APA variation than LAP. APA gradually decreased during the initial phase of the experiment to undetectable levels after the middle of the experiment. Any correlation does not mean causality and the higher coefficient of determination is probably rather a reflection of the clear temporal development in APA. If the AP was produced before the closure of the mesocosm and slowly degraded as discussed above, any connection with the biogeochemical or plankton community must be due to unrelated temporal development. For example, the DIN also decreased over time but was likely not related to the APA.

For the LAP the overall explanatory power by the biogeochemical and plankton community composition was less than for APA, but interestingly the bacterioplankton community composition clearly explained the variability better (38%) than the combined biogeochemical and phytoplankton community (28%). Considering that the bacterial community was not sampled as frequently as the biogeochemical variables and flow cytometer counts, we suspect that the explanatory power would have increased with more frequent sampling. It is likely that bacteria were producing the LAP and some taxa are more reliant on enzyme production for nutrient acquisition than others (Ramin and Allison, 2019). Some dinoflagellates are also known

https://doi.org/10.5194/bg-2022-188
Preprint. Discussion started: 25 October 2022
© Author(s) 2022. CC BY 4.0 License.


524 to produce LAP and most of the mesocosms with high dinoflagellate biomass except M4.
525 However, the phytoplankton community only explained 18% of the variability in LAP, and these
526 dinoflagellates were likely not producing any substantial amount of this enzyme.

527 In conclusion, we found very high levels of LAP (mostly in the range 200 – 800 nmol L^{-1} h^{-1}),
528 which is an order of magnitude higher than most literature data. This is probably linked to the
529 upwelling supporting high levels of microbial activity in combination with the general DIN
530 limitation in the coastal Peruvian upwelling. There was measurable APA at the start of the
531 experiment, but this gradually declined to undetectable levels in all of the mesocosms midway
532 (~30 days) in the experiment. With high concentrations of PO_4^{3-}, low APA is not surprising, and
533 AP is a relatively slowly degrading enzyme that could have been fully dissolved and produced
534 before the closure of the mesocosms. Our statistical mode explained more of the variability of
535 APA (74%) compared with LAP, probably due to its clear temporal development. The
536 bacterioplankton community composition explained best the variability of LAP (38%) compared
537 with the combined biochemical and phytoplankton community model (28%). With more than
538 50% of the variability unaccounted for, we are still missing important pieces of the puzzle
539 understanding the variability in this enzyme. The hydrolysis rates for LAP suggests that pelagic
540 N remineralization supported the relatively high standing stock of primary producers (mostly >4
541 µg chl-*a* L^{-1}) in the mesocosms after N depletion.

542

543

544 Data availability

https://doi.org/10.5194/bg-2022-188
Preprint. Discussion started: 25 October 2022
© Author(s) 2022. CC BY 4.0 License.


All data will be made available on the permanent repository www.pangaea.de after publication.

The DNA sequencing data will be submitted to NCBI SRA (in prep).

Author contribution

Samples were taken by KS, JP, JA, LB, EvdE, MF, NHH, JM and UR. In addition to the sampling crew, further data analysis was conducted by MTCG and MGL. UR developed the experimental design and sampling strategy and coordinated the mesocosm campaign. All co-authors contributed to the data interpretation. KS wrote the manuscript with contributions from all co-authors.

ACKNOWLEDGEMENTS

The experiment was funded through the German Research Foundation (DFG) project: Collaborative Research Centre SFB 754 Climate1074 Biogeochemistry Interactions in the Tropical Ocean. Additional funding came from the Academy of Finland (decision 259164; KS and JP), the EU project AQUACOSM (UR) under grant No. 731065 of the European Union's Horizon 2020 research and innovation programme, the Leibniz Award 2012 of the German Research Foundation (UR) and the Helmholtz International Fellow Award 2015 (JA). This study also used SYKE marine research infrastructure as a part of the Finnish FINMARI consortium. The publication of sequencing data was approved by the Peruvian Ministry of Production with respect to the access and benefit sharing regulations of the Nagoya protocol.

https://doi.org/10.5194/bg-2022-188
Preprint. Discussion started: 25 October 2022
© Author(s) 2022. CC BY 4.0 License.


We thank all participants of the KOSMOS-Peru 2017 study for assisting in mesocosm sampling and maintenance in particular: Andrea Ludwig, Jana Meyer, Jean-Pierre Bednar, Gabriela Chavez, Susanne Feiersinger, Peter Fritsche, Paul Stange, Anna Schukat and Michael Krudewig. We are particularly thankful to the staff of IMARPE for their support during the planning, and to the Marina de Guerra del Perú, the Dirección General de Capitanías y Guardacostas and the Club Náutico Del Centro Naval for their great support. The NMDS plots and GAM models were produced by Dr. Riina Klais-Peets at EcoStat ltd.

REFERENCES

Aldunate, M., De la Iglesia, R., Bertagnolli, A. D., and Ulloa, O.: Oxygen modulates bacterial community composition in the coastal upwelling waters off central Chile, Deep Sea Research Part II: Topical Studies in Oceanography, 156, 68-79, 2018.

Ammerman, J.: Microbial cycling of inorganic and organic phosphorus in the water column, Handbook of methods in aquatic microbial ecology, 1, 649-660, 1993.

Anabalón, V., Morales, C., González, H., Menschel, E., Schneider, W., Hormazabal, S., Valencia, L., and Escribano, R.: Micro-phytoplankton community structure in the coastal upwelling zone off Concepción (central Chile): Annual and inter-annual fluctuations in a highly dynamic environment, Prog Oceanogr, 149, 174-188, 2016.

https://doi.org/10.5194/bg-2022-188
Preprint. Discussion started: 25 October 2022
© Author(s) 2022. CC BY 4.0 License.


584 Arnosti, C.: Microbial extracellular enzymes and the marine carbon cycle, Ann Rev Mar Sci, 3,
585 401-425, 2011.

586 Bach, L. T., Alvarez-Fernandez, S., Hornick, T., Stuhr, A., and Riebesell, U.: Simulated ocean
587 acidification reveals winners and losers in coastal phytoplankton, PloS one, 12, e0188198, 2017.

588 Bach, L. T., Paul, A. J., Boxhammer, T., Esch, E. v. d., Graco, M., Schulz, K. G., Achterberg, E.,
589 Aguayo, P., Aristegui, J., Ayon, P., Banos, I., Bernales, A., Boegeholz, A. S., Chavez, F., Chen,
590 S.-M., Doering, K., Filella, A., Fischer, M., Grasse, P., Haunost, M., Hennke, J., Hernandez-
591 Hernandez, N., Hopwood, M., Igarza, M., Kalter, V., Kittu, L., Kohnert, P., Ledesma, J.,
592 Lieberum, C., Lischka, S., Loescher, C., Ludwig, A., Mendoza, U., Meyer, J., Meyer, J.,
593 Minutolo, F., Cortes, J. O., Piiparinen, J., Sforna, C., Spilling, K., Sanchez, S., Spisla, C., Sswat,
594 M., Moreira, M. Z., and Riebesell, U.: Factors controlling plankton productivity, particulate
595 matter stoichiometry, and export flux in the coastal upwelling system off Peru, Biogeosciences
596 17: 4831-4852, 2020.

597 Badylak, S., Phlips, E. J., and Mathews, A. L.: Akashiwo sanguinea (Dinophyceae) blooms in a
598 sub-tropical estuary: an alga for all seasons, Plankton and Benthos Research, 9, 147-155, 2014.

599 Benitez-Nelson, C. R., and Buesseler, K. O.: Variability of inorganic and organic phosphorus
600 turnover rates in the coastal ocean, Nature, 398, 502-505, 1999.

601 Bolger, A. M., Lohse, M., and Usadel, B.: Trimmomatic: a flexible trimmer for Illumina
602 sequence data, Bioinformatics, 30, 2114-2120, 2014.

https://doi.org/10.5194/bg-2022-188
Preprint. Discussion started: 25 October 2022
© Author(s) 2022. CC BY 4.0 License.


603 Buchan, A., G. R. LeCleir, C. A. Gulvik, and J. M. González. 2014. Master recyclers: Features
604 and functions of bacteria associated with phytoplankton blooms. Nat. Rev. Microbiol. 12: 686–
605 698. doi:10.1038/nrmicro3326.

606 Burley, S. K., David, P. R., Taylor, A., and Lipscomb, W. N.: Molecular structure of leucine
607 aminopeptidase at 2.7-A resolution, Proc Natl Acad Sci, 87, 6878-6882, 1990.

608 Canfield D., Kristensen E., and Thamdrup B.: Aquatic geomicrobiology. Elsevier, 2005.

609 Callbeck, C. M., Lavik, G., Ferdelman, T. G., Fuchs, B., Gruber-Vodicka, H. R., Hach, P. F.,
610 Littmann, S., Schoffelen, N. J., Kalvelage, T., and Thomsen, S.: Oxygen minimum zone cryptic
611 sulfur cycling sustained by offshore transport of key sulfur oxidizing bacteria, Nature
612 communications, 9, 1-11, 2018.

613 Chafee M, Fernàndez-Guerra A, Buttigieg PL, Gerdts G, Eren AM, Teeling H, Amann RI (2017)
614 Recurrent patterns of microdiversity in a temperate coastal marine environment. The ISME J
615 12:237

616 Chavez, F. P., Bertrand, A., Guevara-Carrasco, R., Soler, P., and Csirke, J.: The northern
617 Humboldt Current System: Brief history, present status and a view towards the future, Prog
618 Oceanogr, 79, 95-105, 2008.

619 Christian J.R., Karl D.M.: Bacterial ectoenzymes in marine waters: activity ratios and
620 temperature responses in three oceanographic provinces. Limnol Oceanogr, 40:1042-1049, 1995.

621 Coverly, S., Kérouel, R., and Aminot, A.: A re-examination of matrix effects in the segmented-
622 flow analysis of nutrients in sea and estuarine water, Analytica chimica acta, 712, 94-100, 2012.

https://doi.org/10.5194/bg-2022-188
Preprint. Discussion started: 25 October 2022
© Author(s) 2022. CC BY 4.0 License.


623 Edgar, R. C., Haas, B. J., Clemente, J. C., Quince, C., and Knight, R.: UCHIME improves
624 sensitivity and speed of chimera detection, Bioinformatics, 27, 2194-2200, 2011.

625 Ewing, B., and Green, P.: Base-calling of automated sequencer traces using phred. II. Error
626 probabilities, Genome research, 8, 186-194, 1998.

627 Ewing, B., Hillier, L., Wendl, M. C., and Green, P.: Base-calling of automated sequencer traces
628 usingPhred. I. Accuracy assessment, Genome research, 8, 175-185, 1998.

629 FAO: The state of world fisheries and aquaculture, Food and Agriculture Organization of the
630 United Nations, Rome, 223 pp., 2018.

631 Fischer, M. A., Güllert, S., Refai, S., Künzel, S., Deppenmeier, U., Streit, W. R., and Schmitz, R.
632 A.: Long-term investigation of microbial community composition and transcription patterns in a
633 biogas plant undergoing ammonia crisis, Microbial Biotechnology, 12, 305-323, 2019a.

634 Fischer, M. A., Ulbricht, A., Neulinger, S. C., Refai, S., Waßmann, K., Künzel, S., and Schmitz-
635 Streit, R. A.: Immediate effects of ammonia shock on transcription and composition of a biogas
636 reactor microbiome, Front Microbiol, 10, 2064, 2019b.

637 Garreaud, R. D.: A plausible atmospheric trigger for the 2017 coastal El Niño, International
638 Journal of Climatology, 38, e1296-e1302, 2018.

639 Gier, J., Sommer, S., Löscher, C. R., Dale, A. W., Schmitz-Streit, R., and Treude, T.: Nitrogen
640 fixation in sediments along a depth transect through the Peruvian oxygen minimum zone,
641 Biogeosciences (BG), 13, 4065-4080, 2016.

https://doi.org/10.5194/bg-2022-188
Preprint. Discussion started: 25 October 2022
© Author(s) 2022. CC BY 4.0 License.


642 Graco, M. I., Purca, S., Dewitte, B., Castro, C. G., Morón, O., Ledesma, J., Flores, G., and
643 Gutiérrez, D.: The OMZ and nutrient features as a signature of interannual and low-frequency
644 variability in the Peruvian upwelling system, 2017.

645 Gutiérrez, M., Pantoja, S., Tejos, E., and Quiñones, R.: The role of fungi in processing marine
646 organic matter in the upwelling ecosystem off Chile, Mar Biol, 158, 205-219, 2011.

647 Hauss, H., Franz, J. M., and Sommer, U.: Changes in N: P stoichiometry influence taxonomic
648 composition and nutritional quality of phytoplankton in the Peruvian upwelling, J Sea Res, 73,
649 74-85, 2012.

650 Hoppe, H.-G., Kim, S.-J., and Gocke, K.: Microbial decomposition in aquatic environments:
651 combined process of extracellular enzyme activity and substrate uptake, Appl. Environ.
652 Microbiol., 54, 784-790, 1988.

653 Hoppe, H.-G., Arnosti, C., and Herndl, G.: Ecological significance of bacterial enzymes in the
654 marine environment, Enzymes in the Environment: Activity, Ecology, and Applications, 73-107,
655 2002.

656 Hoppe, H.-G.: Phosphatase activity in the sea, Hydrobiol, 493, 2003.

657 Jeong, H. J., Du Yoo, Y., Park, J. Y., Song, J. Y., Kim, S. T., Lee, S. H., Kim, K. Y., and Yih,
658 W. H.: Feeding by phototrophic red-tide dinoflagellates: five species newly revealed and six
659 species previously known to be mixotrophic, Aquat Microb Ecol, 40, 133-150, 2005.

https://doi.org/10.5194/bg-2022-188
Preprint. Discussion started: 25 October 2022
© Author(s) 2022. CC BY 4.0 License.


660 Kalvelage, T., Lavik, G., Lam, P., Contreras, S., Arteaga, L., Löscher, C. R., Oschlies, A.,
661 Paulmier, A., Stramma, L., and Kuypers, M. M.: Nitrogen cycling driven by organic matter
662 export in the South Pacific oxygen minimum zone, Nature Geosci, 6, 228-234, 2013.

663 Keeling, R. F., Körtzinger, A., and Gruber, N.: Ocean deoxygenation in a warming world, Ann
664 Rev Mar Sci, 2, 199-229, 2010.

665 Kérouel, R., and Aminot, A.: Fluorometric determination of ammonia in sea and estuarine waters
666 by direct segmented flow analysis, Mar Chem, 57, 265-275, 1997.

667 Labry, C., Delmas, D., Youenou, A., Quere, J., Leynaert, A., Fraisse, S., Raimonet, M., and
668 Ragueneau, O.: High alkaline phosphatase activity in phosphate replete waters: The case of two
669 macrotidal estuaries, Limnol Oceanogr, 61, 1513-1529, 2016.

670 Margalef, R., Estrada, M., and Blasco, D.: Functional morphology of organisms involved in red
671 tides, as adapted to decaying turbulence, in: Toxic dinoflagellate blooms, edited by: Taylor, D.
672 L., and Seliger, H. H., Elsevier-North Holland, Amsterdam, 89-94, 1979.

673 Maßmig, M., Lüdke, J., Krahmann, G., and Engel, A.: Bacterial degradation activity in the
674 eastern tropical South Pacific oxygen minimum zone, Biogeosciences, 17, 215-230, 2020.

675 Messié, M., and Chavez, F. P.: Seasonal regulation of primary production in eastern boundary
676 upwelling systems, Prog Oceanogr, 134, 1-18, 2015.

677 Morris, A., and Riley, J.: The determination of nitrate in sea water, Analytica Chimica Acta, 29,
678 272-279, 1963.

https://doi.org/10.5194/bg-2022-188
Preprint. Discussion started: 25 October 2022
© Author(s) 2022. CC BY 4.0 License.


679 Murphy, J., and Riley, J. P.: A modified single solution method for the determination of
680 phosphate in natural waters, Analytica chimica acta, 27, 31-36, 1962.

681 Murphy, K. R., Stedmon, C. A., Wenig, P., and Bro, R.: OpenFluor–an online spectral library of
682 auto-fluorescence by organic compounds in the environment, Analytical Methods, 6, 658-661,
683 2014.

684 Nausch, M.: Alkaline phosphatase activities and the relationship to inorganic phosphate in the
685 Pomeranian Bight (southern Baltic Sea), Aquat Microb Ecol, 16, 87-94, 1998.

686 Nowinski, B., Motard-Côté, J., Landa, M., Preston, C. M., Scholin, C. A., Birch, J. M., Kiene, R.
687 P., and Moran, M. A.: Microdiversity and temporal dynamics of marine bacterial
688 dimethylsulfoniopropionate genes, Env Microbiol, 21, 1687-1701, 2019.

689 Ordination methods, diversity analysis and other functions for community and vegetation
690 ecologists, 2019.

691 Oschlies, A., Brandt, P., Stramma, L., and Schmidtko, S.: Drivers and mechanisms of ocean
692 deoxygenation, Nature Geosci, 11, 467-473, 2018.

693 Pajares, S., Varona-Cordero, F., and Hernández-Becerril, D. U.: Spatial Distribution Patterns of
694 Bacterioplankton in the Oxygen Minimum Zone of the Tropical Mexican Pacific, Microb Ecol,
695 2020.

696 Perry, M.: Alkaline phosphatase activity in subtropical Central North Pacific waters using a
697 sensitive fluorometric method, Mar Biol, 15, 113-119, 1972.

https://doi.org/10.5194/bg-2022-188
Preprint. Discussion started: 25 October 2022
© Author(s) 2022. CC BY 4.0 License.


698 Pruesse, E., Peplies, J., and Glöckner, F. O.: SINA: accurate high-throughput multiple sequence
699 alignment of ribosomal RNA genes, Bioinformatics, 28, 1823-1829, 2012.

700 Rose, C., and Axler, R. P.: Uses of alkaline phosphatase activity in evaluating phytoplankton
701 community phosphorus deficiency, Hydrobiol, 361, 145-156, 1997.

702 Ramin K.I., and Allison S.D.: Bacterial tradeoffs in growth rate and extracellular enzymes. Front
703 Microbiol, 10: 2956, 2019.

704 Schloss, P. D., Westcott, S. L., Ryabin, T., Hall, J. R., Hartmann, M., Hollister, E. B.,
705 Lesniewski, R. A., Oakley, B. B., Parks, D. H., and Robinson, C. J.: Introducing mothur: open-
706 source, platform-independent, community-supported software for describing and comparing
707 microbial communities, Appl Env Microbiol, 75, 7537-7541, 2009.

708 Schulz, K. G., Achterberg, E. P., Arístegui, J., Bach, L. T., Baños, I., Boxhammer, T., Erler, D.,
709 Igarza, M., Kalter, V., Ludwig, A., Löscher, C., Meyer, J., Meyer, J., Minutolo, F., von der Esch,
710 E., Ward, B. B., and Riebesell, U.: Nitrogen loss processes in response to upwelling in a
711 Peruvian coastal setting dominated by denitrification – a mesocosm approach, Biogeosciences,
712 18, 4305–4320, 2021.

713 Schunck, H., Lavik, G., Desai, D. K., Großkopf, T., Kalvelage, T., Löscher, C. R., Paulmier, A.,
714 Contreras, S., Siegel, H., and Holtappels, M.: Giant hydrogen sulfide plume in the oxygen
715 minimum zone off Peru supports chemolithoautotrophy, PloS one, 8, e68661, 2013.

716 Shah, V., Chang, B. X., and Morris, R. M.: Cultivation of a chemoautotroph from the SUP05
717 clade of marine bacteria that produces nitrite and consumes ammonium, The ISME journal, 11,
718 263-271, 2017.

https://doi.org/10.5194/bg-2022-188
Preprint. Discussion started: 25 October 2022
© Author(s) 2022. CC BY 4.0 License.


719 Song, C., Cao, X., Zhou, Y., Azzaro, M., Monticelli, L. S., Maimone, G., Azzaro, F., La Ferla,
720 R. and Caruso, G.: Nutrient regeneration mediated by extracellular enzymes in water column and
721 interstitial water through a microcosm experiment. Sci Tot Env 670: 982-992, 2019.

722 Spilling, K., Camarena-Gómez, M.-T., Lipsewers, T., Martinez-Varela, A., Díaz-Rosas, F.,
723 Eronen-Rasimus, E., Silva, N., von Dassow, P., and Montecino, V.: Impacts of reduced inorganic
724 N: P ratio on three distinct plankton communities in the Humboldt upwelling system, Mar Biol,
725 166, 114, 2019.

726 Stedmon, C. A., and Bro, R.: Characterizing dissolved organic matter fluorescence with parallel
727 factor analysis: a tutorial, Limnology and Oceanography: Methods, 6, 572-579, 2008.

728 Stoecker, D. K., and Gustafson, D. E.: Cell-surface proteolytic activity of photosynthetic
729 dinoflagellates, Aquat Microb Ecol, 30, 175-183, 2003.

730 Thomson, B., Wenley, J., Currie, K., Hepburn, C., Herndl, G. J., and Baltar, F.: Resolving the
731 paradox: continuous cell-free alkaline phosphatase activity despite high phosphate
732 concentrations, Mar Chem, 214, 103671, 2019.

733 Wood, S. N.: Generalized additive models: an introduction with R, CRC press, 2017.

734

735

736

737

https://doi.org/10.5194/bg-2022-188
Preprint. Discussion started: 25 October 2022
© Author(s) 2022. CC BY 4.0 License.


738 Figure legends

739

740 Fig 1. The concentration of dissolved inorganic nitrogen (DIN), phosphate (PO_4^{3-}), dissolved
741 organic nitrogen (DON) and phosphorus (DOP). The red and blue color are the mesocosm bags
742 with deep-water addition with low (closer to shore) and very low (further offshore) oxygen
743 minimum zone (OMZ) signature, respectively. The green dashed lines denote the time of OMZ
744 water addition.

745

746 Fig 2. The fluorescence dissolved organic matter (FDOM) components (C1-C4) during the
747 experiment. The red and blue color are the mesocosm bags with deep-water addition with low
748 (closer to shore) and very low (further offshore) oxygen minimum zone (OMZ) signature,
749 respectively. The green dashed lines denote the time of OMZ water addition.

750

751 Fig 3. The Chlorophyll-*a* (Chl-*a*) concentration (upper graph) and the photochemical efficiency
752 (lower graph). The red and blue color are the mesocosm bags with deep-water addition with low
753 (closer to shore) and very low (further offshore) oxygen minimum zone (OMZ) signature,
754 respectively. The green dashed lines denote the time of OMZ water addition.

755

756

https://doi.org/10.5194/bg-2022-188
Preprint. Discussion started: 25 October 2022
© Author(s) 2022. CC BY 4.0 License.


757 Fig 4. Development of the main groups of phytoplankton enumerated by flow cytometry. The red
758 and blue color are the mesocosm bags with deep-water addition with low (closer to shore) and
759 very low (further offshore) oxygen minimum zone (OMZ) signature, respectively. The green
760 dashed lines denote the time of OMZ water addition.

761

762

763 Fig 5. The bacterial community composition in the 8 mesocosms taken at different time points.
764 In the upper row are mesocosms with deep-water from low OMZ signature (30 m depth) and in
765 the second row with very low OMZ signature (90 m depth). The Y-axis indicates the relative
766 abundance of the bacterial taxa. Only the groups that contributed more than 0.5 % of the total
767 sequences are included and the rest are grouped as “Other Bacteria”. The classification was
768 performed mainly in class, order and genus levels. The abbreviations indicate the main class
769 levels: Alphaproteobacteria (orange shades), Gammaproteobacteria (blue-pink shades),
770 Deltaproteobacteria (green shades), and Bacteroidia (yellow shades) .

771

772 Fig 6. The leucine aminopeptidase (LAP) and cumulative LAP activity. The red and blue color
773 are the mesocosm bags with deep-water addition with low (closer to shore) and very low (further
774 offshore) oxygen minimum zone (OMZ) signature, respectively. The green dashed lines denote
775 the time of OMZ water addition.

776

https://doi.org/10.5194/bg-2022-188
Preprint. Discussion started: 25 October 2022
© Author(s) 2022. CC BY 4.0 License.


777

778 Fig 7. The alkaline phosphatase activity (APA) and cumulative APA. The red and blue color are
779 the mesocosm bags with deep-water addition with low (closer to shore) and very low (further
780 offshore) oxygen minimum zone (OMZ) signature, respectively. The green dashed lines denote
781 the time of OMZ water addition.

782

783

784 Fig 8. Non-parametric multidimensional scaling (NMDS) plots for biochemical, phytoplankton
785 community and bacterioplankton community (upper row). From the NMDS scores, generalized
786 additive models (GAMs) were made (lower two rows) where we used alkaline phosphatase
787 activity (APA) and leucine aminopeptidase (LAP) as dependent variables. The output scores
788 (mds1 and mds2) of the NMDS are depicted in the lower two rows.

789

790

791

https://doi.org/10.5194/bg-2022-188
Preprint. Discussion started: 25 October 2022
© Author(s) 2022. CC BY 4.0 License.

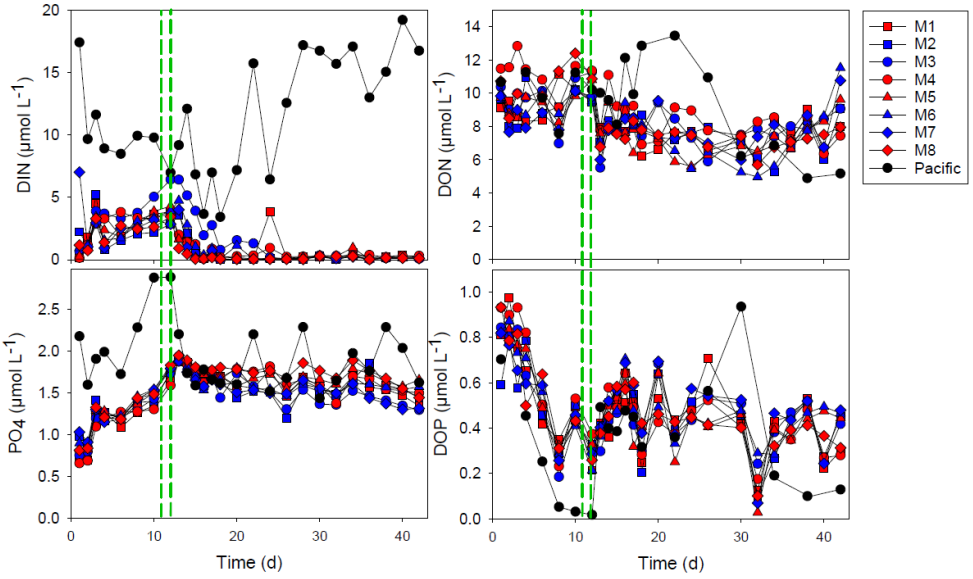

FIG 1

https://doi.org/10.5194/bg-2022-188
Preprint. Discussion started: 25 October 2022
© Author(s) 2022. CC BY 4.0 License.

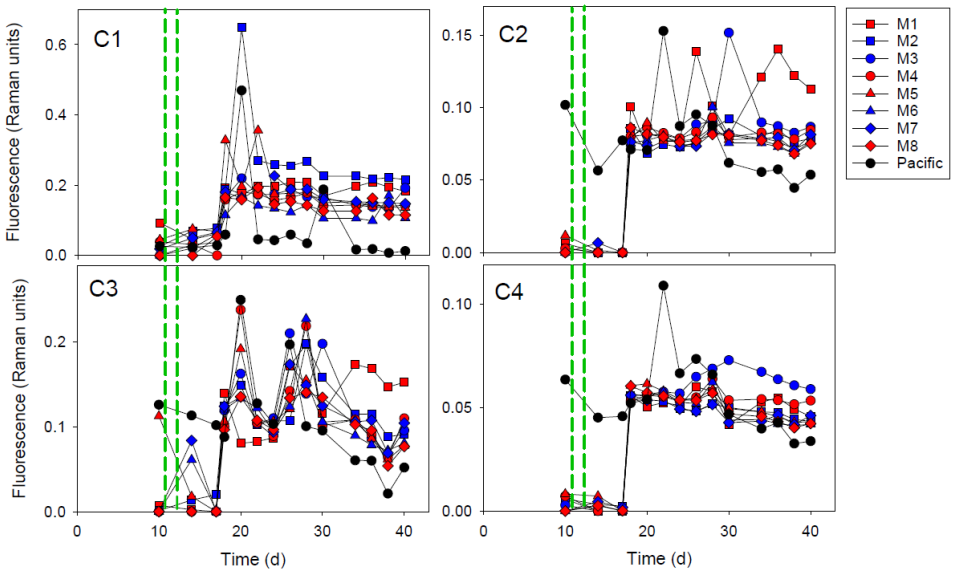

FIG 2

796
797

https://doi.org/10.5194/bg-2022-188
Preprint. Discussion started: 25 October 2022
© Author(s) 2022. CC BY 4.0 License.

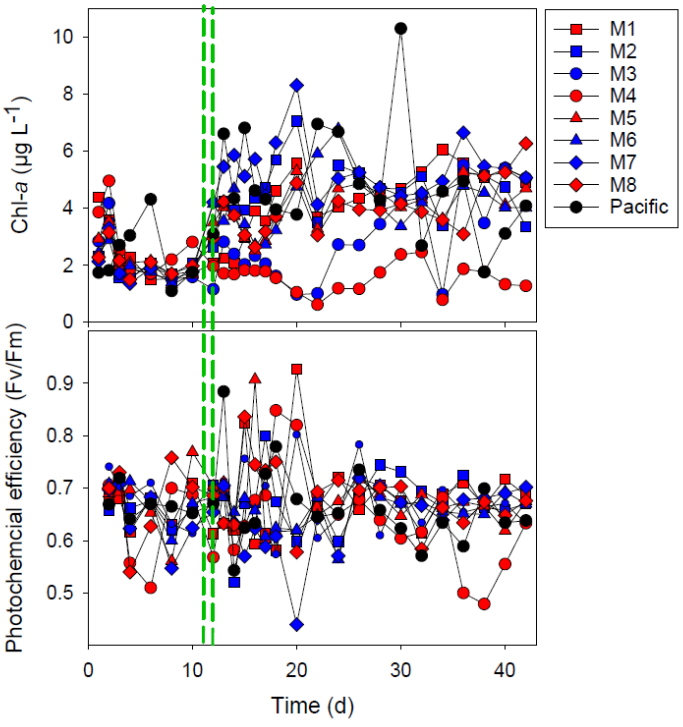

FIG 3

798
799

https://doi.org/10.5194/bg-2022-188
Preprint. Discussion started: 25 October 2022
© Author(s) 2022. CC BY 4.0 License.

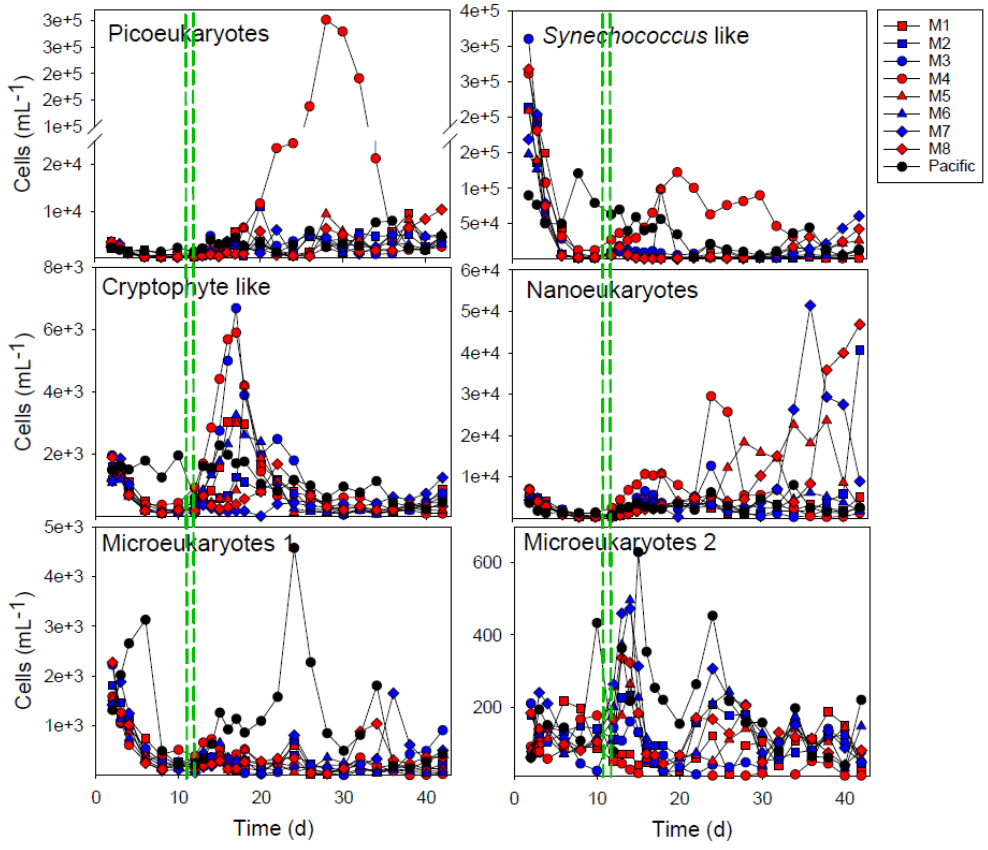

FIG 4

https://doi.org/10.5194/bg-2022-188
Preprint. Discussion started: 25 October 2022
© Author(s) 2022. CC BY 4.0 License.

803

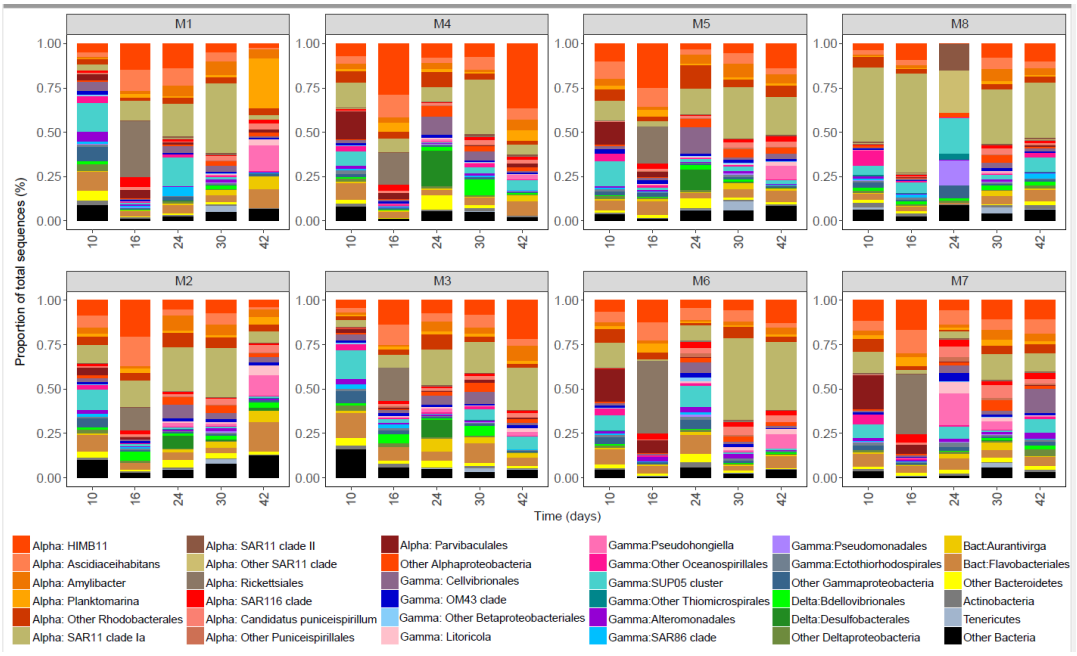

804

805 FIG 5

806

https://doi.org/10.5194/bg-2022-188
Preprint. Discussion started: 25 October 2022
© Author(s) 2022. CC BY 4.0 License.

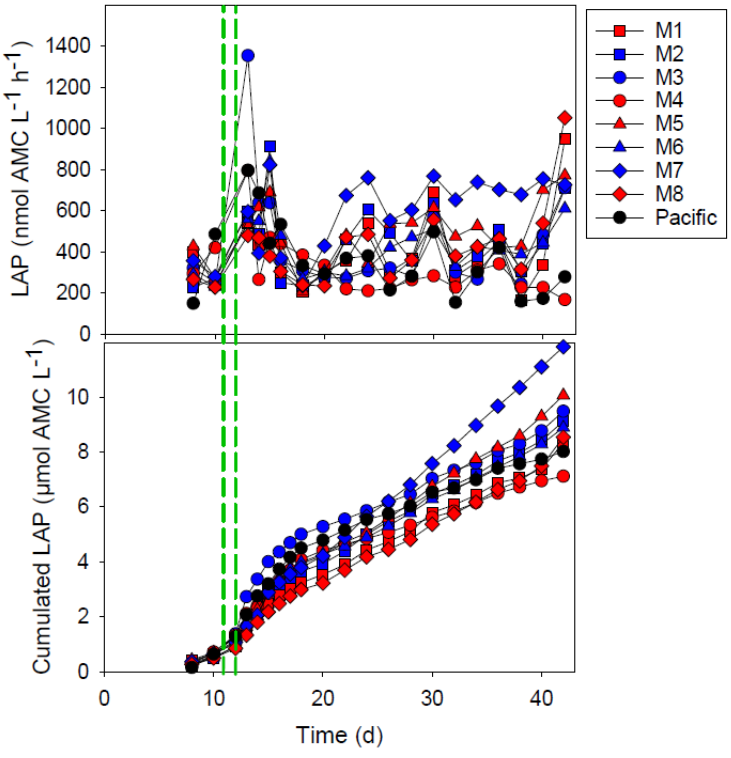

807

808 Fig 6

809

https://doi.org/10.5194/bg-2022-188
Preprint. Discussion started: 25 October 2022
© Author(s) 2022. CC BY 4.0 License.

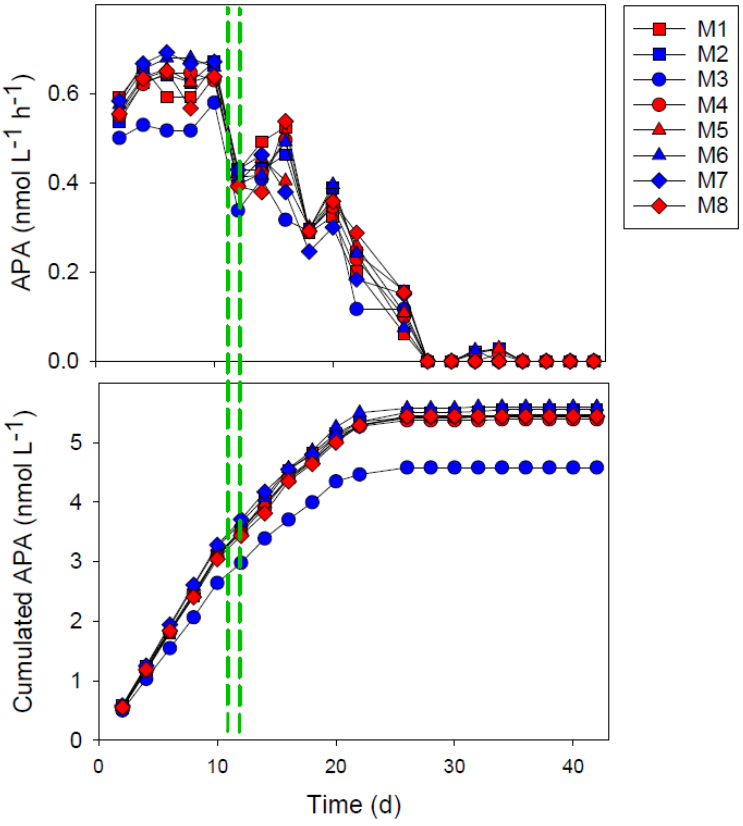

810

811 Fig 7

812

https://doi.org/10.5194/bg-2022-188
Preprint. Discussion started: 25 October 2022
© Author(s) 2022. CC BY 4.0 License.

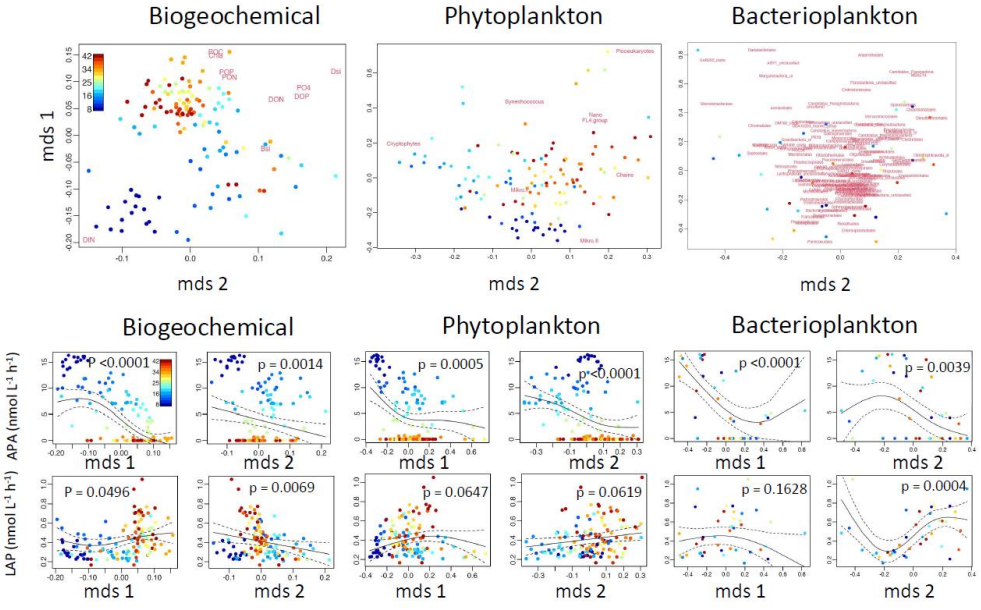

813

814 FIG 8